PERGAMON

Journal of Structural Geology 23 (2001) 715–724

JOURNAL OF STRUCTURAL GEOLOGY

www.elsevier.nl/locate/jstrugeo

The development of flanking folds during simple shear and their use as kinematic indicators

Bernhard Grasemann[a,*], Kurt Stüwe[b]

[a]*Institut für Geologie, University of Vienna, A-1090 Vienna, Austria*
[b]*Institut für Geologie und Paläontologie, University of Graz, A-8010 Graz, Austria*

Received 14 September 1999; accepted 21 June 2000

Abstract

We used a numerical finite element simulation to model the formation of flanking folds around rotating planar structures (e.g. veins, faults or dykes) in a non-linear viscous medium during ideal simple shear. If the planar structure is much more viscous than its host it does not deform and flanking folds with no displacement along the structure develop. Their vergence is consistent with the overall sense of shear. However, if the planar structure is much less viscous than its host, strain is concentrated within the structure and a secondary shear zone is developed in which slip is opposite to the overall sense of shear. Then, flanking folds develop that have a vergence, which is incompatible with the drag on structure. If the deflection of markers is not clearly preserved, then such flanking folds can be easily misinterpreted as shear bands indicating a wrong shear sense. The deflection of the foliation in flanking folds is very similar to deformed asymmetric pull-aparts and can therefore help to interpret these otherwise ambiguous shear sense criteria. Because our model (ideal simple shear boundary conditions) fails to describe back-rotation of planar structures in rocks we speculate that shear band geometries are indicative for general shear.

1. Introduction

1.1. Flanking structures

When the fabric of a rock (e.g. the foliation or lithological layering) is deflected near the margins of a planar structure within the rock (e.g. a fault or a cross cutting vein or dyke) flanking structures will be developed (Grasemann et al., 1999; Passchier, in press). Except for some early descriptions of deflection and/or folding of foliation along dykes and veins (Gayer et al., 1978; Baumann, 1986; Rice, 1986; Passchier and Urai, 1988; Hudleston, 1989), the importance of flanking folds has been appreciated only very recently (e.g. Druguet et al., 1997; Grasemann et al., 1999; Passchier, in press). Some of these authors have illustrated (and warned of) the enormous similarity between different flanking geometries arising from opposite sense of shear. Especially different sense of slip along the planar structure (henceforth called: transecting element, TE) may lead to similar structures, which can be only interpreted kinematically correct if the deflection of the rock (henceforth called: host element, HE) is genetically understood. For example, the difference between extensional shear bands formed in sinistral shear (Fig. 1a) and passively-rotated TE's formed in dextral shear (Fig. 1b) may only be recognizable in the resulting different angles between the HE and the TE (in this case: flanking shear bands and flanking folds respectively; Passchier, in press). Unfortunately, the sense of offset along the TE as well as the deflection of the HE is often difficult to determine, because of the lack of marker horizons (Hudleston, 1989). This problem is closely related to the interpretation of the shear sense of asymmetric boudins and/or foliation boudinage. Depending on the sense of rotation of lozenge-shaped pull-aparts (Fig. 1c and d), almost identical asymmetric boudin geometries may form during dextral or sinistral shear and must therefore be considered as quite ambiguous kinematic indicators (Hanmer, 1986; Goldstein, 1988).

Such geometric similarities may lead (and have led) to grave misinterpretations of the direction of shear sense. If the pull-aparts are ductilely deforming the clarification of the deflection of HE near the necks of the boudins can help to reveal the kinematics of the flow.

In this paper we investigate the development of flanking folds, which are a subset of other flanking structures (Passchier, in press). For our study we use a numerical

* Corresponding author. Fax: +49-131-336-782.
E-mail addresses: bernhard.grasemann@univie.ac.at (B. Grasemann), kurt.stuewe@kfunigraz.ac.at (K. Stüwe).

0191-8141/01/$ - see front matter
PII: S0191-8141(00)00108-5

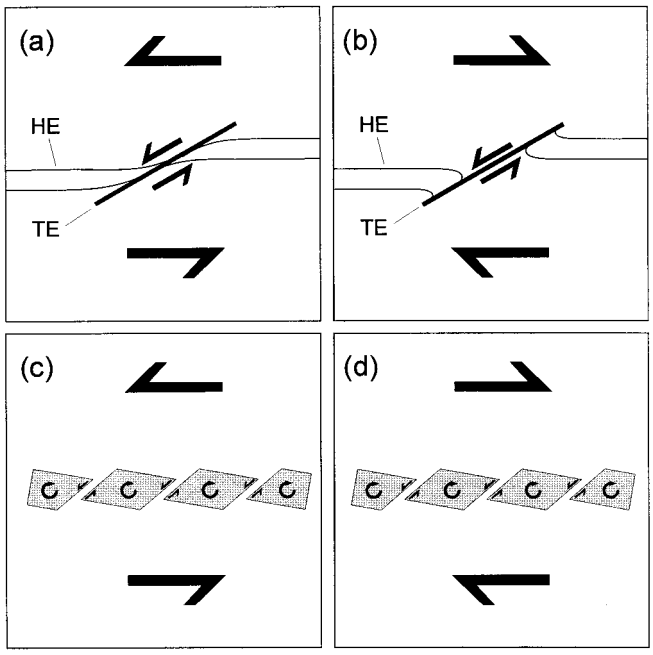

Fig. 1. Similarities and differences between (a) extensional shear bands and (b) flanking folds around a shear zone. Note that the overall shear sense is sinistral in (a) but dextral in (b). Only careful inspection of the deflection of the markers near the shear zone can reveal the correct kinematics. (c) and (d) show both an asymmetric boudinage. In (c) lozenge-shaped boudins are rotating opposite to the sinistral shear sense whereas in (d) the boudins are rotating in the direction of the dextral shear (bookshelf or domino structure). Without deflection of markers the boudins are ambiguous kinematic indicators (Hanmer, 1986; Goldstein, 1988). HE—host element, TE—transecting element (Passchier, in press).

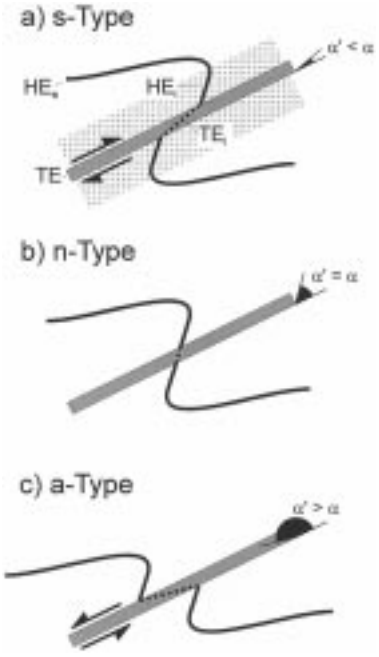

Fig. 2. The nomenclature for different parts of the flanking structure (Passchier, in press) used in the text is llustrated in (a). HE_e—external host element, HE_i—internal host element, TE—transecting element, TE_i—internal transecting element. Depending on the angles α (angle between TE and TE_i before deformation) and α' (angle between TE and TE_i after deformation), three geometric types of flanking structures are distinguished: (a) s-Type with synthetic displacement ($\alpha' < \alpha$); (b) n-Type with no displacement ($\alpha' = \alpha$); (c) a-Type with antithetic displacement ($\alpha' > \alpha$). In all three examples the overall sense of shear is dextral. In this paper we discuss only n-Type and a-Type flanking structures.

model with ideal simple shear boundary conditions and compare our results with a range of field examples. We investigate the displacement and strain field within and outside the TE during progressive deformation as a function of the rheology contrast between the TE and the HE. As the paper aims to clarify some fatal misinterpretations of shear sense direction, we begin with a clear definition of the terminology.

1.2. Definition of Terminology

In the discussion below it will be important to discriminate not only between the host element HE and the transecting element TE (Passchier, in press), but also between the deflected host element near the margin of the TE which is call the *internal host element* HE_i, and the *external host element* HE_e not influenced by the TE (Fig. 2a). We also discern between the rotation of the TE itself and the rotation of elements within TE, which are called *internal transecting element* TE_i. Depending on the angles α (angle between TE and TE_i before deformation) and α'(angle between TE and TE_i after deformation), three geometric types of flanking structures are distinguished (Fig. 2): (a) s-Type with synthetic displacement ($\alpha' < \alpha$); (b) n-Type with no displacement ($\alpha' = \alpha$) and (c) a-Type with antithetic displacement ($\alpha' > \alpha$).

Although we use the original definition of s-, n- and a-Type flanking folds (Passchier, in press), we avoid confusion with the definition of syn- and antithetic (Stewart

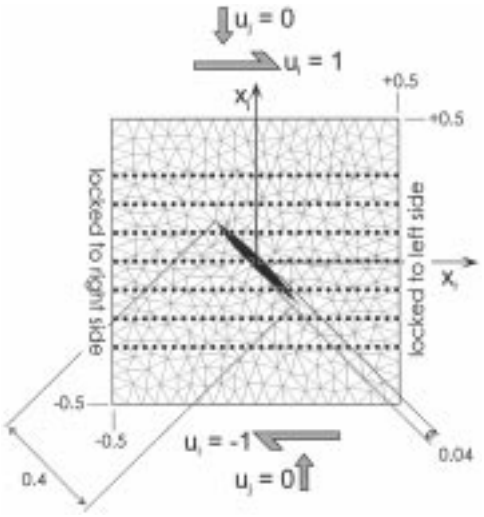

Fig. 3. Model setup of the starting geometry and boundary conditions for the finite element model calculations (for detailed descriptions see text).

and Argent, 2000) by referring to the original definition of Cloos (1928). We use *co-shearing* for the shear sense of secondary shear zones, which have the same sense of displacement as the first order shear zone. Likewise, secondary shear zones with an opposite displacement are *counter-shearing*. Correspondingly, we use *co-rotating* for objects rotating in the same direction as the rotational component of simple shear and *counter-rotating* for objects rotating against the shear sense (G. Oertel, pers. comm.).

Furthermore, we use the classification of asymmetric pull-aparts of Hanmer (1986). However, we use it in a much broader sense (Jordan, 1991; Swanson, 1992) and define all boudins, pinch and swells and foliation boudinages (Platt and Vissers, 1980), which rotate in the direction of shear as Type I and against the shear as Type II.

Throughout the paper we follow the conventions of classical structural geology textbooks and define all positive angles as counterclockwise. Dextral shear zones have a negative shear strain γ (Ramsay and Huber, 1983).

2. Numerical techniques

We investigate the development of flanking folds around TE that formed prior to the development of the folds during ideal simple shear, using the two-dimensional finite element model BASIL of Barr and Houseman (1996). Flanking folds are an inherently two-dimensional structure and BASIL is therefore well-suited for their dynamic interpretation. We assume a non-linear viscous rheology for both the TE and the HE in which stress is proportional to strain rate raised by some power. In a general form, such a constitutive relationship may be written by relating the components of deviatoric stress and strain rate by:

$$\tau_{ij} = B\dot{E}^{\left(\frac{1}{n}-1\right)}\dot{\varepsilon}_{ij} \tag{1}$$

where τ_{ij} are the deviatoric components of the stress tensor, $\dot{\varepsilon}_{ij}$ are the components of the strain rate tensor and $\dot{E}$ is the second invariant of the strain rate tensor. The pre-exponent proportionality constant B incorporates all material constants and temperature dependent terms (England and McKenzie, 1982). The i and j subscripts represent the two Cartesian directions. Strain rate is defined in terms of the components of velocity u, in the x_i- and x_j-direction:

$$\dot{\varepsilon}_{ij} = \frac{1}{2}\left[\frac{\partial u_i}{\partial x_j} + \frac{\partial u_j}{\partial x_i}\right]. \tag{2}$$

The rheology contrast between TE and HE was implemented by using different values of B for the host element and the transecting element. The stress exponent n for both TE and HE was assumed to be the same. The results presented below are for $n = 1$. Then, Eq. (1) reduces to a linear relationship between stress and strain rate in which B is the proportionality constant, called viscosity (equivalent to a Newtonian fluid). Then, with $B = 100$, TE is hundred times as viscous (strong) as the HE and for $B = 0.01$ TE is hundred times less viscous (weaker) than the matrix, which has a normalized viscosity of 1. Thus, the viscosity B of the TE is also the viscosity- or rheology-contrast between the TE and the HE. For $B = 1$, there is no rheological difference between the TE and the HE and the entire model is equivalent to ideal simple shear conditions. Rheology contrasts larger than 100 or smaller than 0.01 did not show any change in the results. Results for up to $n = 5$ were calculated, but vary kinematically so little from the results presented here, that it is not justified to discuss them.

The two-dimensional calculations were done using BASIL by solving the force balance equations in two dimensions:

$$\frac{\partial}{\partial x_j}\tau_{ij} + \frac{\partial}{\partial x_i}p = 0 \tag{3}$$

where summation is over the i and j indices and p is the pressure. The strain during progressive deformation was calculated with Eq. (1) and assuming plane strain deformation. After every time step velocity **u** and the pressure p are recorded at every node of the grid shown in Fig. 3.

2.1. Initial and boundary conditions

The initial and boundary conditions are illustrated in Fig. 3. The TE has the dimension of 0.4 length and 0.04 width (colored black in Fig. 3), relative to a square box with the dimensionless length 1. Only flanking folds around TE that are initially oriented at 135 degrees to the shear zone boundary and the HE were modeled (Durney and Ramsay, 1973). This starting condition is analogous to the formation of tension gashes, veins or fractures that were initially oriented parallel to the shortening instantaneous stretching axis of isochoric plane strain simple shear flow (Passchier, 1997).

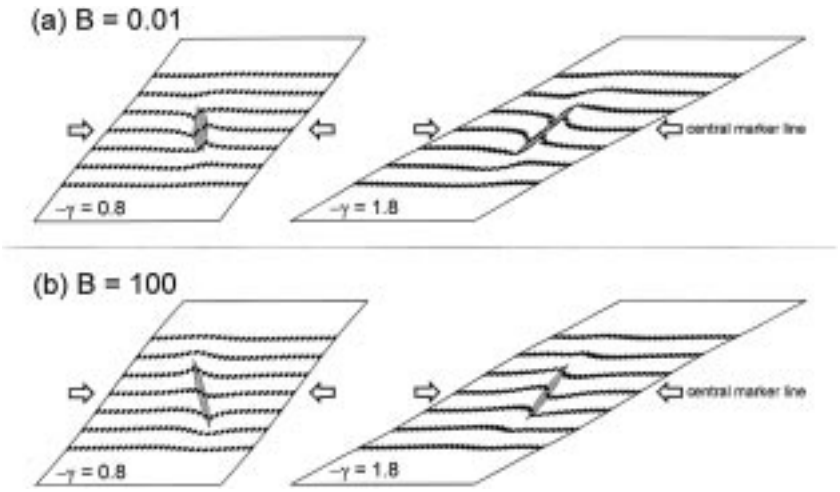

Fig. 4. Results of the model calculations showing the strain during formation of flanking folds: (a) for $B = 0.01$, (b) for $B = 100$. Small circular passive strain markers initially arranged in rows and columns (Fig. 3) are shown after deformation for $-\gamma = 0.8$ and $-\gamma = 1.8$, respectively. The imaginary lines connecting the center of the strain ellipses represent passive marker lines whereas the ellipticity indicate strain.

The surface of the TE is made up of two circle segments. The grid was generated with a self-meshing routine using Delauney triangles with a minimum angle of 20°. We have tested the robustness of the results for mesh-size and for the dimensions of the TE and found that a finer grid or narrower TE width does not influence the numerical results.

Boundary conditions were used that approximate ideal simple shear in a long shear zone. For this we used displacement boundary conditions at the top and bottom of the box in Fig. 3. There, the x_j-component of the velocity is 0. The x_i-component of the velocity is 1 on the top boundary and -1 on the bottom boundary. As such a shear strain $-\gamma$ of 2 is achieved at time step 1. On the sides we assumed that all velocities and stresses on the left boundary are identical to those on the right boundary. Thus, the model geometry has a ring shape describing an infinite shear zone and no side-boundary conditions need to be implemented.

3. Results

In the model setup described above a-Type flanking folds develop by counter-shearing slip along the TE if TE is less viscous than the HE ($B < 1$). If the TE is stronger than the host element ($B > 1$) n-Type flanking forms by relative rotation of the TE with respect to the HE (Fig. 4). The result is best visualized in the form of small circular passive strain markers initially arranged in rows and columns (Fig. 3). After deformation the imaginary lines connecting the center of the strain ellipses represent passive marker lines whereas the ellipticity indicates strain (Fig. 4). Depending on the viscosity ratio between the modeled TE and HE different geometries of flanking folds develop, but dextral shear sense will always result in z-shaped flanking folds, which have a vergence consistent with the shear sense of the shear zone. Instructive video files of the modeled progressive deformation can be downloaded from our web site: http://bigaxp. geologie.univie.ac.at/flanking_folds

3.1. Weak transecting elements ($B = 0.01$)

This numerical experiment describes natural examples where a TE is much weaker than its host element and is illustrated in Fig. 4a and Fig. 5a. This may be given by an open fracture which allows nearly free slip during rotation of the fracture (Hudleston, 1989) or when the transecting element is a ductile shear zone in which flow is concentrated (Gayer et al., 1978; Baumann, 1986).

After onset of deformation the TE changes its shape with decreasing ellipticity (i.e. shortened and thickened) until it is aligned perpendicular to the shear zone (Fig. 4a, $-\gamma = 0.8$). After rotating through this position, where the incremental longitudinal strain of a material line is zero (Ramsay and Huber, 1983), the ellipticity of TE increases (i.e. it stretches and thins). The displacement along TE is counter-shearing and consequently marker lines are offset across TE. Therefore, this model always results in a-Type flanking folds. The amount of offset is largest in the center of TE and diminishes towards zero at the tips of TE. Considering TE as a shear zone and neglecting the external spin of this shear zone, TE initially suffers convergent transcurrence, which changes to divergent transcurrence (Marrett and Peacock, 1999) after TE is rotated through its position perpendicular to the shear zone boundary. As a result of this complex counter-shearing along TE, the HE around the vein is deflected into flanking folds. The strain within the short limbs of the flanking folds (i.e. HE_i) is markedly reduced. According to the diminishing amount of offset along TE, the amplitude of the flanking folds decreases towards the tip of TE. Characteristically, the marker line above and below TE forms a monoclinal fold with an opposite vergence than that of the flanking folds. As a consequence marker lines are

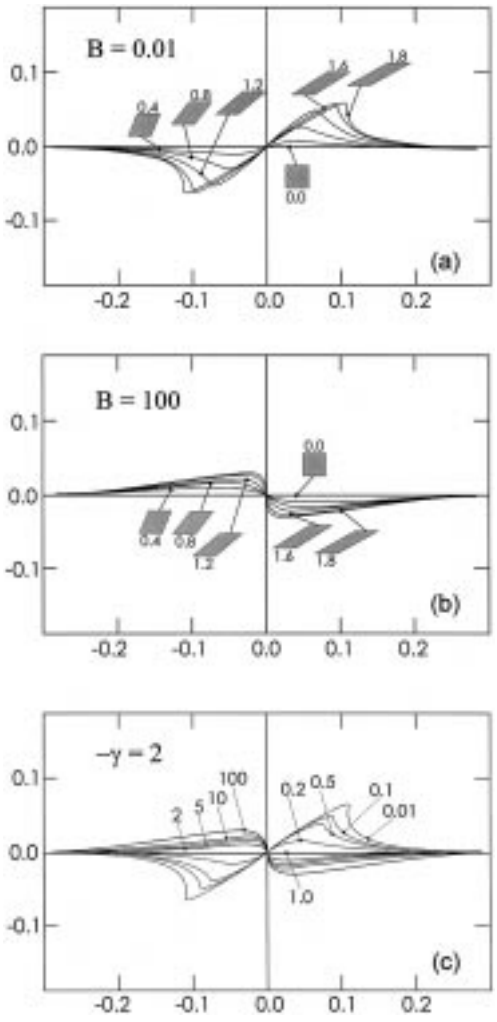

Fig. 5. Shape of central marker lines, which were oriented parallel to the shear zone boundary through the center of TE before deformation. (a) Marker lines for $B = 0.01$ during increasing shear strain ($0 < -\gamma < 1.8$). (b) Marker lines for $B = 100$ during increasing shear strain ($0 < -\gamma < 1.8$). (c) Marker lines for $0.01 < B < 1$ (dashed curves) and $1 < B < 100$ (solid curves) for a shear strain of $-\gamma = 2$.

converging at the tip of the TE, where flanking folds and monoclinal folds meet (Fig. 4a, $-\gamma = 1.8$).

Fig. 5a shows the central marker line, which was oriented parallel to the shear zone boundary through the center of TE before deformation, during increasing shear strain ($0 < -\gamma < 1.8$). The interlimb angles of the flanking folds are decreasing with increasing shear strain due to progressive co-rotation of the HE_i marker lines. The rotation of the TE_i material line is more complex reflecting the complicated interplay between rotational non-coaxial flow and spin of the TE shear zone (rotational/non-coaxial/spinning shear zone in the sense of Passchier, 1986). Up to shear strains of $-\gamma \sim 1.2$ the material line is counter-rotating because of the counter-shear along TE. The rotation rate of the TE_i has an opposite sense and is higher than the rotation rate of TE. However, at this stage the TE_i material line is already at a low angle to the long axis of TE, whereas the angle between the shear zone boundary and TE is still much higher. Therefore, at higher shear strains ($\sim -\gamma > 1.2$) the external rotation rate of the TE shear zone is larger and consequently the internal TE_i is co-rotating within the external reference frame.

3.2. Strong transecting elements ($B = 100$)

These numerical experiments describe natural examples where the TE is much more competent than HE and is illustrated in Fig. 4b and Fig. 5b. This situation may be given when the transecting element is a tension gash filled by some rheologically strong material or by a strong intrusive dyke. Note that this model can be also applied to geological examples where a more competent rim is attached to the TE (e.g. Passchier, in press). In this special case of a very high viscosity contrast ($B = 100$) the TE is rigid and does not change its shape during deformation. Consequently the strain markers within TE remain unit circles, they are not offset, and the model always results in n-Type flanking folds. Similar to the experiment with a weaker TE (Fig. 4a), the marker lines above and below the TE form monoclinal folds (Fig. 4b). However, in the models with a strong TE the monoclinal folds and the flanking folds have the same vergence.

Fig. 5b shows the central marker line, which was oriented parallel to the shear zone boundary through the center of TE before deformation, during increasing shear strain ($0 < -\gamma < 1.8$). The interlimb angles of the flanking folds are decreasing with increasing shear strain due to progressive passive co-rotation of TE_i.

3.3. Variable viscosity contrast between TE and HE

Sections 3.1 and 3.2 have described the extremes of rheology contrast between host- and transecting-elements. However, in many natural examples the rheology of TE and HE may be quite similar, for example when TE is a quartz vein emplaced in a HE which is a quartz-rich felsic gneiss. In order to illustrate flanking folds for rheologically similar HE and TE Fig. 5c shows the shape of flanking folds for the rheology contrast range $0.01 < B < 100$. It may be seen that all qualitative characteristics described for $B = 0.01$ hold for $B < 1$ and those described for $B = 100$ hold for $B > 1$. It may also be seen that the width of HE_i is roughly constant, regardless of B. Interestingly, there is a similar structural development for high viscosity contrasts during increasing strain, as there is for high strains during increasing viscosity contrast (compare Fig. 5a,b and 5c). Thus, flanking folds around very strong TE ($B = 100$) at a shear strain of $-\gamma = 1$ will have an almost identical geometry to flanking folds around less strong TE ($B = 5$) at a shear strain of $-\gamma = 2$. Correspondingly, flanking folds around extremely weak TE ($B = 0.01$) at $-\gamma = 1$ are very similar in geometry to flanking folds around TE that were only half as strong as HE ($B = 0.5$) at $-\gamma = 2$. As a consequence, we suggest that care must be taken when interpreting strain from the

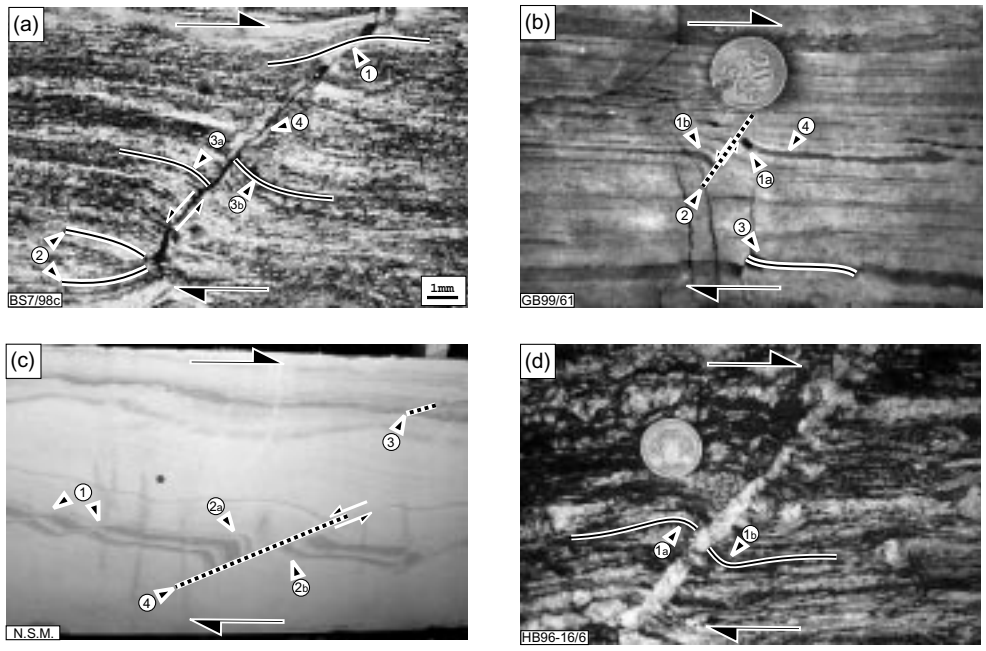

Fig. 6. Natural examples of flanking folds: (a) Thin section (crossed polarized light) of a pure quartz mylonite cut parallel to the lineation and normal to the foliation from the Schober Group, Austria (N46°55.311′, E12°43.338′). The shape-preferred orientation of fine dynamically recrystallized quartz grains reveals a dextral sense of shear. The deflection of the foliation around a rotated fracture shows many similarities with the result of the model calculations of a-Type flanking folds shown in Fig. 4a: [1] Monoclinal fold at the tip of TE with a vergence opposite to the shear sense. [2] Converging foliation near the tip of TE, [3a] Antiformal and [3b] synformal flanking fold with a vergence consistent to the sense of shear. [4] Dynamically recrystallized quartz indicating counter-shearing in the co-rotating TE. (b) Calcite mylonite from a major normal fault in Naxos, Greece (N37°11.393′, E25°30.919′). During a late stage of deformation the metamorphic layering is boudinaged by fractures [2], which are co-rotating during progressive deformation resulting in the formation of a-Type flanking folds [1a, b] and Type I boudinage [3] (compare Fig. 8a). (c) Block of Laaser Marble cut parallel to the lineation and normal to the foliation (quarry in Vintschgau, Italy; photo courtesy of N. Mancktelow, ETH Zürich). Whereas the structures at [1] could be misinterpreted as shear bands or Type II boudinage (compare Fig. 8b) indicative for a sinistral sense of shear, the strongly developed fold-train at [2a and b] reveals a-Type flanking fold with an overall dextral shear. Note that the graphitic markers at [2b] make the typical s-shape of co-rotating Type I boudins (compare Fig. 8a). The dextral shear sense is furthermore confirmed by a small thrust developed at [3]. d) n-Type flanking fold [1a, b] around a rotated quartz vein within the Main Central Thrust zone in the Sutlej Valley, India (N31°21.023′, E77°23.143′). The deflection of the mylonitic foliation is very similar to the model results of Fig. 4b, indicating that the vein has been stronger during this stage of deformation.

geometry of a flanking fold, unless the rheology contrast between HE and TE can be estimated (Treagus, 1999).

4. Comparison with natural examples

4.1. Examples of weak transecting elements

Fig. 6a shows a thin section of a pure quartz mylonite from the Schober Group (Austria Austria, N46°55.311′, E12°43.338′) with fine dynamically-recystallized grains. The quartz grains have a well-developed shape and crystal preferred orientation indicating a dextral sense of shear. The mylonitic foliation (HE) is transected by a fracture (TE) with a sinistral slip. Below and more clearly above the fracture the HE forms a monoclinal fold with an opposite vergence than the overall sense of shear ([1] in Fig. 6a). Approaching the tip of the fracture the foliations form an antiform on the upper end and a synform on the lower end consistent with the counter-shearing slip on the fracture. As a result of this syn- and antiformal deflection of HE the foliation converges at the tips of TE ([2] in Fig. 6a). The z-shape antiform–synform fold train ([3a and b] in Fig. 6a) developed towards the center of the fracture have axial planes dipping in the same direction as the fault. However, the deflection of HE is apparently incompatible with the sinistral slip of the fault. This structure is interpreted as an a-Type flanking fold, which formed in the vicinity of a co-rotating fracture. Probably this fracture developed at a high angle to the shear zone and rotated clockwise during a still ductile dextral non-coaxial deformation. Ductile sinistral slip along the fracture is furthermore confirmed by dynamically-recrystallizing quartz ([4] in Fig. 6a).

The resulting deflection of the mylonitic foliation is nearly identical to the results of the model calculations of Fig. 4a. Note that in the absence of a clear deflection of the foliation in the central part of the fracture the flanking structure could be easily misinterpreted as a shear band, indicating an opposite (i.e. sinistral) shear sense.

As a second example, Fig. 6b shows a calcite mylonite from a major normal fault in Naxos (Greece, N37°11.393′, E25°30.919′) with an unambiguous north-directed shear

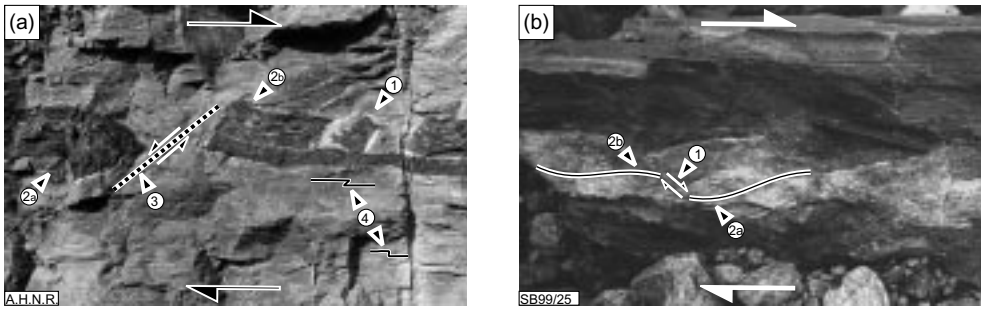

Fig. 7. (a) Type I boudinaged metabasic dyke in paragneisses within the Kalak Nappe Complex (Finnmark, N-Norway; photo courtesy of H. Rice, University of Vienna). Whereas the rotated pull-apart at [1] could be easily confused with a Type II counter-rotating boudin revealing a sinistral sense of shear, the antiform of an a-Type flanking fold at [2a] suggests dextral kinematics. The metabasic dyke segment at [2b] makes the typical s-shape of co-rotating Type I boudins (compare Fig. 8a). The deformed boudins are separated by counter shearing zones of distributed strain [3]. Dextral displacement is also confirmed by abundant z-shaped folds [4]. (b) Type II boudinage of a pegmatite within the Austroalpine Crystalline (Schober Group, Austria; loose block at N46°55.967′, E12°42.584′). The co-shearing movement between the pull-aparts is recorded by shear-band type deflection of the internal foliation [2a, b] consistent with the sense of shear at [1] (compare Fig. 8b).

sense (N is right in Fig. 6b). During a late stage of deformation the metamorphic layering is boudinaged by fractures ([2] in Fig. 6b), which are co-rotating during progressive deformation resulting in the formation of a-Type flanking folds ([1a, b] in Fig. 6b). Qualitatively the shape of the dark slightly more competent layer ([4] in Fig. 6b) is comparable with the form of the central marker line in Fig. 5a after a shear strain of $-\gamma = 1.2$. The dark more competent layer ([3] in Fig. 6b) forms a typical Type I boudinage (compare Fig. 8a) discussed below in more detail.

Fig. 6c illustrates the importance of carefully investigating the deflection of HE in order to interpret the structure with an example of a-Type flanking folds in the Laaser Marble (Vintschgau, Italy, Fig. 6c). In the left part of the block ([1] in Fig. 6c), black graphitic layers in the nearly pure white marble are offset by shear zones, which—following classical structural geology text books—would be interpreted as shear bands with a Riedel like geometry (Platt 1984), indicating a sinistral sense of shear. However, following the graphitic layers to the right side of the block a sinistral shear zone is associated with a fold train verging towards the right of the picture ([2a and b] in Fig. 6c). Again it is suggested that these folds are a-Type flanking folds, developed near a dextral rotating TE with a counter-shearing slip. Note that the shape of the graphitic layer truncated by two faults with sinistral offset on each side ([2b] in Fig. 6c) is very similar to the Type I boudins in Fig. 7a, discussed below. The overall dextral sense of shear is further supported by a small thrust developed in the upper right part of the marble block ([3] in Fig. 6c).

Both, the numerical model results (Fig. 4) and these natural examples of a rather homogeneous fine-grained quartz mylonite (Fig. 6a) and of a pure marble (Fig. 6c) as well as observations from glaciers (Hambrey and Milnes, 1975) confirm that flanking folds do not need a pronounced pre-existing anisotropy like a foliation defined by alignment of micas in the HE in order to develop around a TE.

Exceptionally beautiful examples of a-Type flanking folds (and correct kinematic interpretation!) are given in Swanson (1998) using asymmetric pull-aparts for estimating minimum shear strains during non-coaxial deformation. Figure 71B in Swanson (1998) reveals a reversal of the antiformal bending of the flanking fold into a small syncline immediately adjacent to the TE consistent with a counter shearing drag along TE. This drag effect is also seen in Fig. 6c [1] and may complicate the correct kinematic interpretation. Comparing these natural examples with our modeled central marker lines (Fig. 5c), this drag effect may be a function of the viscosity contrast between TE and HE.

4.2. Examples of strong transecting elements

The examples discussed above showed a-Type flanking folds with deflection of the markers similar to the results of the model calculations illustrated in Fig. 4a and 5a. In contrast, quartz-filled rotated extension gashes in mylonitic orthogneisses from the Main Central Thrust in the NW-Himalayas (Grasemann et al., 1999) indicate that the TE, probably with an attached rim (HE_i), was more competent during deformation than HE_e (Fig. 6d). This can best be seen from a direct comparison between Fig. 4b and 6d. In this case n-Type flanking folds formed by relative rotation of quartz veins probably together with attached rims being more competent than the host rock material during this stage of the deformation. A high angle between the HE_i and TE is preserved (i.e. ~105° in Fig. 6d). Under favorable conditions this angle may represent the initial opening angle even if the angle between HE_e and TE is low (i.e. ~45° in Fig. 6d) and may be used as a quantitative kinematic indicator (Grasemann et al., 1999). Comparison with the results of the model calculations where the TE is undeformable (i.e. $B = 100$) reveals that folding is just an effect of passive rotation of the TE_i (and HE_i) and a counter-shearing drag effect between TE (and HE_i) and HE_e.

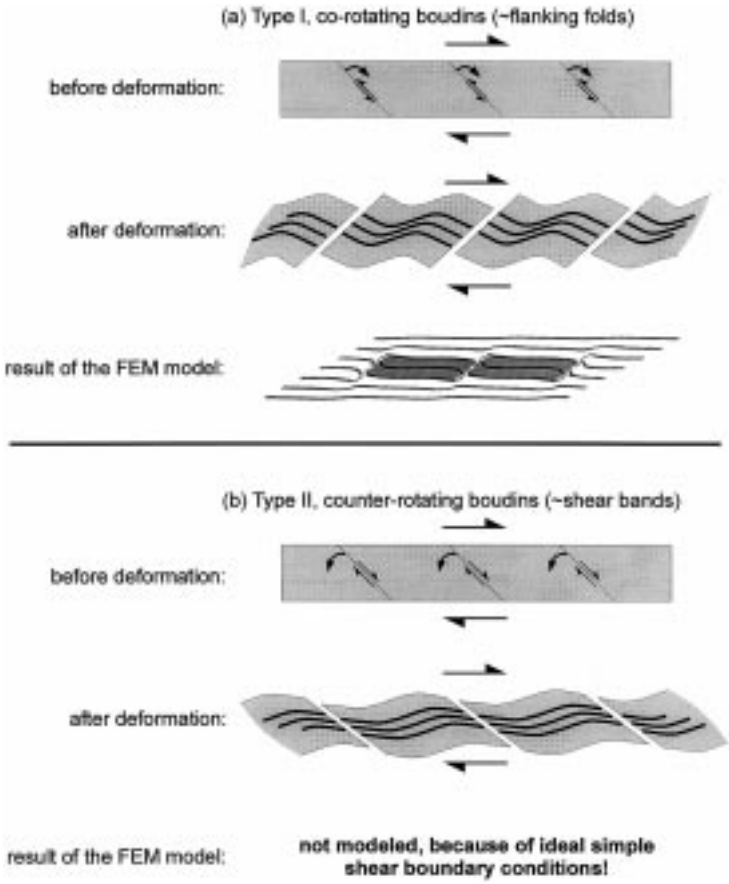

Fig. 8. (a) Co-rotating (Type I) and (b) counter-(Type II) boudinage (Hanmer 1986, Goldstein 1988). If the pull-aparts are rigid and reveal no internal deformation, these types of boudins are ambiguous kinematic indicators. However, if the boudinaged layer is deformed, the sense of rotation of the fracture separating the boudins can be derived. Note, that the geometry of Type I is very similar to the a-Type flanking folds modeled in Fig. 4a.

5. Discussion

5.1. A cautious note on flanking structures as kinematic indicators.

The boundary conditions used in the presented models for the development of flanking folds are ideal simple shear, isochoric plane-strain flow in the far field. However, Baumann (1986) showed that a-Type flanking folds, which are nearly identical to our modeled structures, can also develop under pure shear isochoric plane-strain flow. The model setup and starting geometry assumed a less competent TE oriented at an intermediate position between the two orthogonal eigenvectors of flow. During pure shear deformation non-coaxial strain is concentrated within TE rotating towards the stretching eigenvector and resulting in an a-Type flanking fold. The results of Baumann (1986) and our work can be best compared using the concept of perturbation strain (Baumann, 1986; Mancktelow, 1991): Finite deformation can be viewed to be composed of (i) the average, homogeneous part of deformation as defined by the boundary conditions and (ii) the component by which local deformation is perturbed from this. In case of the pure shear model of Baumann (1986) the non-coaxial perturbation strain of the rotating TE has to be balanced along the margins of TE with a rotational deformation but with a different sign in order to compensate the overall average homogeneous coaxial deformation. In case of our dextral simple shear model the sinistral general shearing perturbation deformation of the co-rotating TE has to be balanced along the margins of TE with a dextral general shear deformation in order to compensate the overall dextral homogeneous ideal simple shearing. Therefore the kinematic of the flow has to be constrained independently by different shear sense indicators in order to interpret flanking structures correctly (e.g. Figs. 6 and 7). However, flanking structures are still very useful because they bear important information about the flow geometry, which will be subject of further models including general shear boundary conditions.

5.2. A cautious note on asymmetric boudinage as kinematic indicators.

A familiar example that may be easily misinterpreted kinematically is the development of structures around a TE during boudinage. Our numerical model does not include anisotropies or more competent layers within the

HE—as they occur during boudinage. However, the striking similarities of our model results and natural examples of boudinaged layers (compare Figs. 6–8), merits a short discussion. Asymmetric boudinage or "back-rotation" of boudins and pinch and swells are frequently used shear sense criteria (e.g. Cloos, 1947; Ramberg, 1955; Hanmer, 1986; Goldstein, 1988; Jordan, 1991). Strömgård (1973) investigated the stress field and the factors that may lead to the formation of asymmetric lozenge-shaped pull-aparts. However, crucial for the quantitative kinematic interpretation is whether the boudins are co- (Type I) or counter-rotating (Type II). In the absence of a characteristically deformed marker line (compare Fig. 1c and d) this may be a difficult task and therefore it has been suggested that lozenge-shaped rotated pull-aparts are quite ambiguous kinematic indicators (Hanmer, 1986; Goldstein, 1988; Jordan, 1991). However, if the boudinaged layer is deformed, the deflection of marker lines along the shear fracture separating the pull aparts may help to reveal the sense of rotation.

In Type I co-rotating boudins, the fracture separating the boudins is co-rotating as well, resulting in a counter-shearing slip. The resulting deflection of the markers within the boudins is very similar to the results of the presented model calculations, where a weaker TE is co-rotating during simple shear deformation (Fig. 8a). Thus this type of boudinage could be interpreted as an a-Type flanking fold where the marker lines are displaced along TE in a different sense but where the deflection of HE forms an anti-/synform fold train with a vergence consistent with the overall shear sense. Beautiful natural examples together with an analogue model are given in Fig. 3b and 6 in Hanmer (1986). The close relationship of Type I boudinage to flanking folds is further supported by published superb examples of co-rotating foliation boudinage (figures 9a and 11d in Swanson, 1992).

Another example of an easily misinterpreted boudinage structure is shown in Fig. 7a. This shows a metabasic dyke boudinaged in paragneisses from the Kalak Nappe (Finnmark Norway). First investigations of the boudinage ([1] in Fig. 7a) suggest that fracturing of the metabasic dyke and clockwise counter-rotation of the pull aparts (Type II) indicate sinistral sense of shear. However, a closer inspection of the left part of the picture reveal an antiformal fold at the right end of a boudin ([2a] in Fig. 7a) with a vergence consistent with a dextral sense of shear. Likewise, in continuation of the dyke to the right, the left end of the next boudin shows a slight tendency to deform into a synform ([2b] in Fig. 7a). These observations suggests that the dyke, although fractured, was still able to deform after separating into single pull-aparts and that the fractures initially at a high angle have been clockwise co-rotated in an overall dextral shear ([3] in Fig. 7a) resulting in Type I boudinage. Note that many small-scale z-shaped folds within the paragneisses confirm a dextral shear sense ([4] in Fig. 7a).

In Type II counter-rotating boudins, the fracture separating the boudins is counter-rotating as well, resulting in a co-shearing slip (Fig. 8b). The geometry, the deformation of the pull-aparts and the deflection of markers are very similar to back-rotated oblique shear bands (Swanson, 1992) or ecc-structures (Platt, 1984; Malavielle, 1987; Jordan, 1991). Contrary to the Type I, the markers are deflected along the fracture separating the boudins, which is consistent with the co-shearing slip on it. Many excellent examples of this deflection and deformation of boudins with co-shearing shear band geometries exist (e.g. figures 7 and 8 in Malavielle, 1987).]. Fig. 7b shows a Type II boudinage of a pegmatite within the Austroalpine Crystalline (Schober Group, Austria; loose block at N 46°55.967′, E12°42.584′). The co-shearing movement between the pull-aparts is recorded by shear-band type deflection of the internal foliation ([2a, b] in Fig. 7b) consistent with the sense of shear ([1] in Fig. 7b).

In the presented model calculations with ideal simple shear boundary conditions the TE is always co-rotating and therefore we failed to reproduce counter-rotating and co-shearing TE. Therefore, our model supports the conclusions of Jordan (1991) that counter-rotation of lozenge-shaped boudins with shear band geometries are a typical feature of transpression zones formed by general shear. A more detailed investigation of the mechanism leading to flanking shear bands or Type II boudinage has to be done by expanding our numerical model to general shear boundary conditions.

6. Conclusions

The model calculations presented here reproduce successfully a-Type and n-Type flanking folds, which closely resemble natural examples. From comparison of the natural examples with the numerical modeled structures the following can be concluded:

The recognition of a-Type flanking folds or shear bands requires close inspection of the deflection of markers along TE. In absence of a clear preservation of the deflection of HE_i, especially in the central part of TE, both structures can be easily confused. Confusion of flanking folds and shear bands results in a wrong interpretation of the kinematic frame.

Co- (Type I) and counter-rotating (Type II) boudinaged competent but deformable layers, pinch and swells and foliation boudinage have many similarities to flanking structures. The deflection of marker lines is distinctly different for both types: (i) Type I boudinage results in deflection of markers, which is identical to the presented numerical model of a-Type flanking folds when TE is less competent than HE. The deflection of HE_i is inconsistent with the counter-shearing slip on TE but the associated flanking folds have a vergence consistent with the overall sense of shear. (ii) Deflection of markers in Type II boudinage results in typical shear band geometries. The recognition of the

deflection of markers within such asymmetric pull-aparts is essential for the correct interpretation of the shear sense.

Our model calculations with ideal simple shear boundary conditions was unable to reproduce counter-rotating TE and therefore supports the conclusions of Jordan (1991) that counter-rotation of lozenge-shaped boudins with shear band geometries are a typical feature of transpression zones formed by general shear.

The development of the a- and n-Type flanking folds do not need an anisotropic HE (e.g. foliation) in order to develop but can readily form in homogeneous media in the vicinity of the rotating TE: (i) a-Type flanking folds develop along a counter-shearing TE with free-slip or incompetent TE filling material; (ii) n-Type flanking folds develop by passive co-rotation when the TE_i and sometimes an attached rim of HE_i are more competent than the HE_e.

Acknowledgements

G. Houseman, T. Barr and L. Evans are thanked for their abundant help with learning BASIL. H. Rice and N. Mancktelow are thanked for some of the photo material shown in Figs. 6 and 7 and many fruitful discussions about flanking structures. N. Mancktelow is thanked for sending us a copy of the PhD thesis of M. Baumann. BG acknowledges support from the Austrian "Fonds zur Förderung der wissenschaftlichen Forschung" (FWF grant P-14129-GEO and P-13227-GEO) and the Hochschaljubilaumsstiftung der Stadt Wein. KS was supported by FWF project P-12846-GEO. We thank Erich Draganits, Gerhard Wiesmayr, Helmuth Sölva, Florian Fusseis, Ulli Exner for fruitful discussions and Cees Passchier for sending us a copy of his manuscript about "Flanking Structures" before publication.

References

Barr, T.D., Houseman, G.A., 1996. Deformation fields around a fault embedded in a non-linear ductile medium. Geophysical Journal International 125, 473–490.

Baumann, M.T., 1986. Verformungsverteilung an Scherzonenenden: Analogmodelle und natürliche Beispiele. Unpublished PhD thesis, Universität Zürich.

Cloos, H., 1928. ber antithetische Bewegungen. Geologische Rundschau 19, 246–251.

Cloos, H., 1947. Boudinage. Transactions American Geophysical Union 28, 626–632.

Druguet, E., Passchier, C.W., Carreras, J., Victor, P., Den Brock, S., 1997. Analysis of a complex high-strain zone at Cap de Creus, Spain. Tectonophysics 280, 31–45.

Durney, D.W., Ramsay, J.G., 1973. Incremental strains measured by syntectonic crystal growth. In: De Jong, K.A., Scholten, R. (Eds.), Gravity and Tectonics. Wiley, New York, pp. 67–96.

England, P.C., McKenzie, D., 1982. A thin viscous sheet model for continental deformation. Geophysical Journal of the Royal Astronomical Society 70, 295–321.

Gayer, R.A., Powell, D.B., Rhodes, S., 1978. Deformation against metadolerite dykes in the Caledonides of Finnmark, Norway. Tectonophysics 46, 99–115.

Goldstein, A.G., 1988. Factors affecting the kinematic interpretation of asymmetric boudinage in shear zones. Journal of Structural Geology 10, 707–715.

Grasemann, B., Fritz, H., Vannay, J.C., 1999. Quantitative kinematic flow analysis from the Main Central Thrust Zone (NW-Himalaya, India): implications for a decelerating strain path and the extrusion of orogenic wedge. Journal of Structural Geology 21, 837–853.

Hambrey, M.J., Milnes, A.G., 1975. Boudinage in glacier ice—some examples. Journal of Glaciology 14, 383–393.

Hanmer, S., 1986. Asymmetrical pull aparts and foliation fish as kinematic indicators. Journal of Structural Geology 8, 111–122.

Hudleston, P.J., 1989. The association of folds and veins in shear zones. Journal of Structural Geology 11, 949–957.

Jordan, P.G., 1991. Development of asymmetric shale pull-aparts in evaporite shear zones. Journal of Structural Geology 13, 399–409.

Malavielle, J., 1987. Kinematics of compressional and extensional ductile shearing deformation in a metamorphic core complex of the northeastern Basin and Range. Journal of Structural Geology 9, 541–554.

Mancktelow, N.S., 1991. The analysis of progressive deformation from an inscribed grid. Journal of Structural Geology 13, 859–864.

Marrett, R., Peacock, D.C.P., 1999. Strain and stress. Journal of Structural Geology 21, 1057–1063.

Passchier, C.W., 1986. Flow in natural shear zones—the consequences of spinning flow regimes. Earth and Planetary Science Letters 77, 70–80.

Passchier, C.W., 1997. The fabric attractor. Journal of Structural Geology 19, 113–127.

Passchier, C.W. Flanking structures. Journal of Structural Geology, in press.

Passchier, C.W., Urai, L., 1988. Vorticity and strain analysis using the Mohr diagrams. Journal of Structural Geology 10, 755–763.

Platt, J.P., 1984. Secondary cleavages in ductile shear zones. Journal of Structural Geology 6, 439–442.

Platt, J.P., Vissers, R.L.M., 1980. Extensional structures in anisotropic rocks. Journal of Structural Geology 2, 397–410.

Ramberg, H., 1955. Natural and experimental boudinage and pinch and swell structure. Journal of Geology 63, 512–526.

Ramsay, J.G., Huber, M.I., 1983. The Techniques of Modern Structural Geology—1: Strain Analysis. Academic Press, London, pp. 1–308.

Rice, A.H.N., 1986. Structures associated with superimposed inhomogeneous shearing of basic dykes from Finnmark, Norway. Tectonophysics 128, 61–75.

Stewart, S.A., Argent, J.D., 2000. Relationship between polarity of extensional fault arrays and presence of detachments. Journal of Structural Geology 22, 693–712.

Strömgård, K.E., 1973. Stress distribution during deformation of boudinage and pressure shadows. Tectonophysics 16, 215–248.

Swanson, M.T., 1992. Late Acadian-Alleghenian transpressional deformation: evidence from asymmetric boudinage in the Casco Bay area, coastal Maine. Journal of Structural Geology 14, 323–341.

Swanson, M.T., 1998. Asymmetric boudinage in mylonitic gneisses. In: Snoke, A.W., Tullis, J., Todd, V.R. (Eds.), Fault-related Rocks. Princeton University Press, New Jersey, pp. 246–247.

Treagus, S.H., 1999. Are viscosity ratios of rocks measurable from cleavage refraction? Journal of Structural Geology 21, 895–901.